# Nickel Confined in the Interlayer Region of Birnessite: an Active Electrocatalyst for Water Oxidation

Akila C. Thenuwara, Elizabeth B. Cerkez, Samantha L. Shumlas, Nuwan H. Attanayake,
Ian G. McKendry, Laszlo Frazer, Eric Borguet, Qing Kang, Richard C. Remsing,
Michael L. Klein, Michael J. Zdilla, and Daniel R. Strongin*

Abstract: We report a synthetic method to enhance the electrocatalytic activity of birnessite for the oxygen evolution reaction (OER) by intercalating Ni^{2+} ions into the interlayer region. Electrocatalytic studies showed that nickel (7.7 atomic %)-intercalated birnessite exhibits an overpotential (η) of 400 mV for OER at an anodic current of 10 mA cm^{-2}. This η is significantly lower than the η values for birnessite (η ≈ 700 mV) and the active OER catalyst β-Ni(OH)$_2$ (η ≈ 550 mV). Molecular dynamics simulations suggest that a competition among the interactions between the nickel cation, water, and birnessite promote redox chemistry in the spatially confined interlayer region.

Converting sunlight to useful forms of energy, such as electrical and chemical energy, has the potential to help eliminate the fossil fuel dependence of mankind.[1–6] From this standpoint, designing cheap, efficient, and robust catalysts that can facilitate the splitting of water to oxygen and hydrogen is a worthwhile goal that will potentially pave the path for efficient conversion of solar energy to chemical energy. The splitting of water [Eq. (1)] is thermodynamically uphill and a kinetically hindered reaction, which has a high energetic penalty without a catalyst.[7]

$$H_2O_{(l)} \rightarrow \tfrac{1}{2} O_{2(g)} + H_{2(g)}, \qquad \Delta G = +237\ kJ\ mol^{-1} \qquad (1)$$
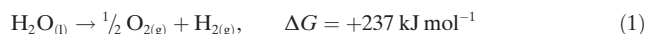
Inspired by the ability of manganese-bearing photosystem II (PS-II) to split water, there have been numerous studies that have utilized manganese-containing compounds as homogeneous and/or heterogeneous catalysts for the oxygen evolution reaction (OER).[8–13]

Birnessite is a naturally occurring manganese oxide mineral that is ubiquitous in soils, nodules, and stream deposits.[14,15] The material is composed of 2D-layers of edge-sharing manganese octahedra (MnO$_6$).[10,14,15] Owing to the presence of both Mn^{3+} and Mn^{4+} within the structure, the overall 2D-like layered structure has a net negative charge. Thus, charge neutrality is usually provided by positively charged alkali metal ions, such as K$^+$ or Na$^+$, in the interlayer region between the MnO$_2$ sheets.[14–17] In general, the interlayer region of birnessite not only contains alkali metal ions, but also contains a confined layer of water, resulting in an interlayer spacing of ≈ 0.7 nm. A recent molecular dynamics (MD) simulation study suggested that the confined interlayer region of birnessite containing metal cations and water leads to unique water structuring that is incommensurate with water–water hydrogen bonding, resulting in frustration of water molecules between the shared cation hydration shells that enhances the rates of interlayer electron transfer reactions beyond standard theoretical expectations.[18]

We hypothesized that the catalytic activity of birnessite for water oxidation could be enhanced by incorporating an already active OER catalytic material into its interlayer region. The model system used to test this hypothesis was potassium birnessite with an intercalated Ni-hydroxide. Ni-hydroxide has been shown in prior studies to be an excellent electocatalyst for OER.[19] In this study, we determined how the OER activity of birnessite intercalated with Ni compared to birnessite and Ni-hydroxide alone.

Herein, we report that the nickel hydrazine complex [Ni(N$_2$H$_4$)$_x$(H$_2$O)$_y$]$^{2+}$ can be used to efficiently transport Ni^{2+} into the interlayer region of potassium-birnessite (see the Supporting Information for more details). Intercalation of Ni^{2+} was confirmed with X-ray diffraction (XRD), Raman spectroscopy, and X-ray photoelectron spectroscopy (XPS). We found that birnessite intercalated with Ni is a more active electrocatalyst for water oxidation compared to nickel hydroxide or birnessite alone.

Scanning electron microscopy (SEM) and transmission electron microscopy (TEM) were performed on birnessite before and after nickel intercalation (Figure 1 and Supporting Information, Figure S1), where the latter material is hereafter referred to as Ni^{2+}/birnessite. A comparison of the micrographs for birnessite and Ni^{2+}/birnessite showed no significant changes in the flower-like morphology of birnessite. Inductively coupled plasma optical emission spectroscopy (ICP-

[*] A. C. Thenuwara, E. B. Cerkez, S. L. Shumlas, N. H. Attanayake,
I. G. McKendry, Dr. L. Frazer, Dr. E. Borguet, Dr. Q. Kang,
Dr. R. C. Remsing, Dr. M. L. Klein, Dr. M. J. Zdilla, Dr. D. R. Strongin
Department of Chemistry, Temple University
1901 N. 13th Street, Philadelphia, PA 19122 (USA)
E-mail: dstrongi@temple.edu

A. C. Thenuwara, S. L. Shumlas, N. H. Attanayake, I. G. McKendry,
Dr. L. Frazer, Dr. E. Borguet, Dr. Q. Kang, Dr. R. C. Remsing,
Dr. M. L. Klein, Dr. M. J. Zdilla, Dr. D. R. Strongin
Center for the Computational Design of Functional Layered Materials
(CCDM) (USA)

Dr. R. C. Remsing, Dr. M. L. Klein
Institute for Computational Molecular Science, Temple University
1925 N. 12th St, Philadelphia, PA 19122 (USA)

Dr. L. Frazer
Present address: School of Chemistry, UNSW
Sydney NSW 2052 (Australia)
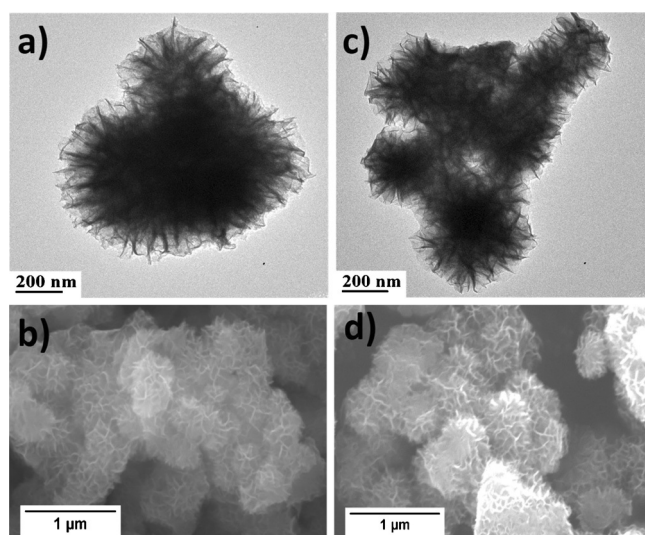
Figure 1. Electron micrographs of Ni^{2+}/birnessite (Ni 6.1%): a) TEM and b) SEM. Images of pristine birnessite: c) TEM and d) SEM.

OES) and energy dispersive spectroscopy (EDS) showed that the concentration of nickel in Ni^{2+}/birnessite (after a 10 min exposure to the Ni-hydrazine complex) was 6.1 atomic%. Also, EDS mapping suggested that the Ni was evenly distributed throughout the Ni^{2+}/birnessite structure (Figure S2).

Based on the shift of the (001) Bragg reflection in the XRD, the interlayer spacing of birnessite decreased from 7.27 Å to 7.17 Å for Ni^{2+}/birnessite (Figure 2a). This observation was consistent with prior research from our laboratory, which showed that the intercalation of copper into the birnessite interlayer resulted in a similar decrease in the interlayer spacing.[13] As a control experiment, birnessite was exposed to hydrazine in the absence of nickel. This circumstance led to significant structural changes, likely owing to a redox reaction of hydrazine with birnessite [Eq. (2)] to form tetragonal Mn_3O_4 (Figure S3). However a prior study reported that exposure of hydrazine to MnO_2 would form MnOOH.[20]

$$2 N_2H_{4(l)} + 12 MnO_{2(s)} \rightarrow 2 N_{2(g)} + 4 Mn_3O_{4(s)} + 4 H_2O_{(l)} \qquad (2)$$
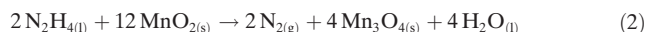
This chemistry was absent when Ni^{2+} was present in the solution, presumably owing to hydrazine complexation with Ni^{2+}. We suspect the majority of the Ni^{2+}-hydrazine stayed complexed in solution and prevented any major structural changes of the birnessite.

Analysis of XRD data (Figure 2b) showed that, with an increased amount of intercalated Ni^{2+}, the interlayer spacing of birnessite decreased from 7.17 (6.1 atomic% Ni) to 7.07 Å for 7.7 atomic% Ni^{2+}/birnessite (30 min exposure to Ni-hydrazine complex). Electron microscopy results from 7.7 atomic% Ni^{2+}/birnessite also showed that there were no significant morphological differences relative to birnessite (Figure S1). No change in the interlayer spacing was observed when birnessite was exposed to only hydrazine; instead, Mn_3O_4 was formed (Figure 2a). Therefore, this decreasing
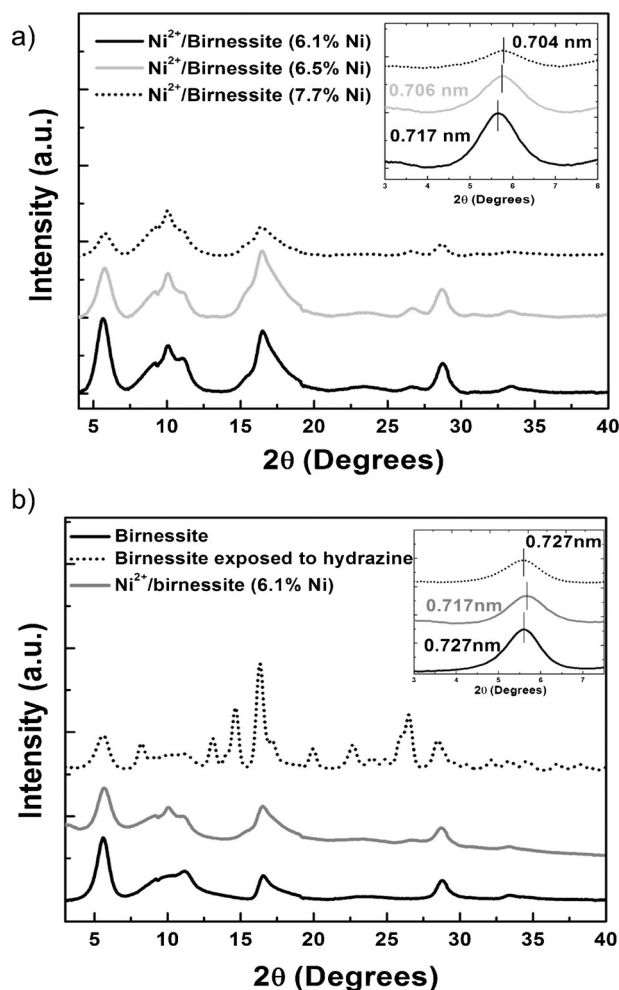
Figure 2. XRD spectra: a) birnessite, birnessite exposed to hydrazine, and Ni^{2+}/birnessite. b) Ni^{2+}/birnessite with varying amounts of intercalated Ni. Inset shows the localized XRD patterns for the (001) reflection that corresponds to the interlayer spacing.

interlayer spacing with exposure to the Ni^{2+}-hydrazine complex is attributed to the increasing amount of intercalated Ni.

The structure of Ni^{2+}/birnessite was also investigated with Raman spectroscopy, which is sensitive to the short range order of materials. Birnessite exhibits two primary Raman modes at ≈ 575 and 646 cm^{-1}.[21–23] Figure S4 shows that both birnessite and birnessite exposed to hydrazine exhibited similar Raman spectra. However, the reduction in the intensity of 575 cm^{-1} mode after hydrazine exposure can be attributed to an increase in Mn^{3+}, which likely formed through a reaction of birnessite with hydrazine (Reaction 2).[23] For Ni^{2+}/birnessite, significant broadening of the two peaks (575 cm^{-1} and 646 cm^{-1}) was observed, and this experimental observation is likely due to some disruption of the Mn–O bonding in the sheets. Prior studies revealed a similar broadening for birnessite that had undergone lithium and copper intercalation.[13,23]

The XPS spectra shown in Figure S5 (XPS Ni 2p region) indicate that intercalated Ni exists as Ni^{2+} in the birnessite interlayer. Examination of the O 1s region (Figures S5 and S6), as well as the Ni 2p region of Ni-hydroxide and Ni-oxide

© 2016 Wiley-VCH Verlag GmbH & Co. KGaA, Weinheim

standards suggests that intercalated nickel has more Ni-hydroxide character than Ni-oxide character.[24] The role that is played by the Ni-hydrazine complex ($[Ni(N_2H_4)_x(H_2O)_y]^{2+}$) is difficult to ascertain, especially because mixed water/hydrazine coordination of nickel is expected in solution, as suggested by simulation results (Figure S9). It may be that in these mixed compositions, positively charged complexes shuttle nickel into the negatively charged interlayer to form Ni^{2+}/birnessite. The absence of nitrogen in Ni^{2+}/birnessite (from XPS) suggested that Ni-hydrazine complex decomposed during the transfer of Ni into the interlayer region. The fate of the hydrazine is not known, but it does not appear to result in any structural changes of the birnessite host material. EDS experiments showed that all of the potassium ions, initially in the birnessite, were removed after the exposure of the material to the Ni-hydrazine complex. This observation indicates that Ni^{2+} ions entering the interlayer region result in the expulsion of interlayer K^+, owing to charge neutrality considerations. This experimental observation is additional strong evidence for the contention that Ni^{2+} resides in the interlayer region of Ni^{2+}/birnessite.

Electrocatalysis studies indicated that the activity of Ni^{2+}/birnessite for OER was superior to the activity exhibited by birnessite and β-$Ni(OH)_2$ (Figure 3). In particular, at a current
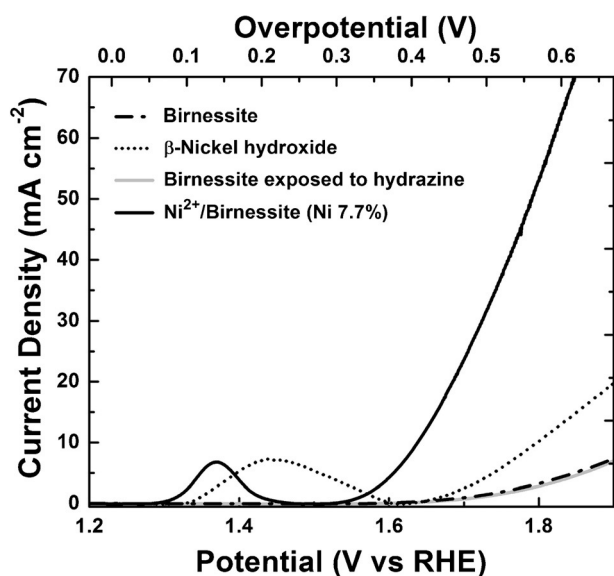
Figure 3. Polarization curves for birnessite, β-$Ni(OH)_2$, birnessite exposed to hydrazine, and Ni^{2+}/birnessite. Ni^{2+}/birnessite shows an enhanced activity relative to β-$Ni(OH)_2$ and birnessite. Data for Ni^{2+}/birnessite and β-$Ni(OH)_2$ were acquired after 100 cycles.

density of 10 mA cm^{-2}, the overpotential (η) values for water oxidation on Ni^{2+}/birnessite, β-$Ni(OH)_2$, and birnessite were 400, 550, and 700 mV, respectively. Furthermore, the polarization curves obtained for birnessite and birnessite exposed to hydrazine showed the same OER activity, thus we can conclude that formation of the Mn_3O_4 phase did not improve catalysis. As shown in Figure 4, OER activity systematically rose with the amount of intercalated nickel. The 7.7 atomic % Ni^{2+}/birnessite catalyst showed the highest OER activity and
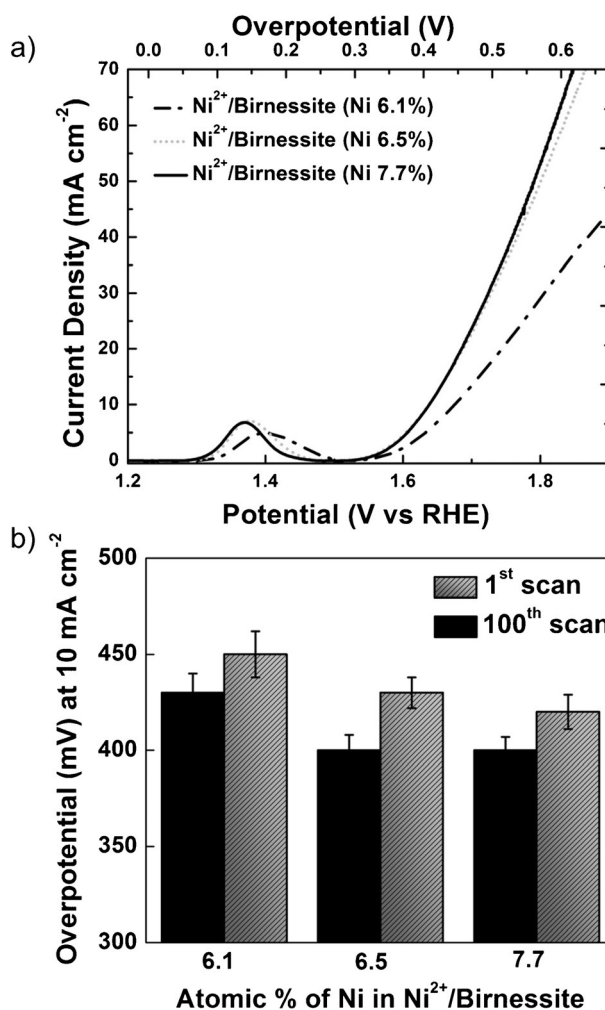
Figure 4. a) Polarization curves for Ni^{2+}/birnessite with varying amounts of Ni. b) Comparison of overpotentials to reach 10 mA cm^{-2} for Ni^{2+}/birnessite with increasing electrochemical cycles.

exhibited an overpotential of 400 mV and a Tafel slope of 60 mV/dec. This Tafel slope of 60 mV/dec is on par with precious metal OER catalysts (for example, IrO_2; see Table S1). The drastic improvement of the Tafel slope from 243 (birnessite) to 60 mV/dec (Ni^{2+}/birnessite) can be attributed to a change in the rate-determining step (RDS) of OER kinetics. Higher Tafel slopes (>120 mV/dec) are typically associated with water adsorption on the catalytic site being the RDS, while lower Tafel slopes (≈ 40 mV/dec) have been suggested to indicate that O–O bond formation is the RDS.[25,26] The change of Tafel slope in our study upon Ni^{2+} intercalation suggests that that interlayer Ni is acting as an active site for OER in Ni^{2+}/birnessite. Additionally, the overpotential (to produce 10 mA cm^{-2}) was observed at 1.68 V versus RHE ($\eta = 450$ mV) for the first electrochemical cycle, but after an increasing number of cycles (Figure 4b) decreased to 1.63 V versus RHE ($\eta = 400$ mV). This activation with cycling is commonly seen in nickel-based electrocatalysts, and is widely accepted to be the result of $Ni^{III}O$-(OH) formation.[19,27] Electrochemical impedance spectroscopy (EIS) further supported this notion, where a reduction in

charge transfer resistance was observed in Ni^{2+}/birnessite with increasing electrochemical cycles (Figure S10). We also observed an oxidative peak associated with the conversion of Ni^{2+} to Ni^{3+} at 1.37 V versus RHE, which provided evidence for the formation of Ni^{3+} as an intermediate[19] redox active species during OER.

Table 1 illustrates the enhanced electrocatalytic activity of Ni^{2+}/birnessite in terms of turnover frequencies (TOF) and

Table 1: Summary of OER activities and atomic ratios from ICP-OES and EDS.

Catalyst	Intercalated Ni atomic %	TOF [s^{-1}] at $\eta = 0.40$ V	Mass activity [A g^{-1}] at $\eta = 0.40$ V	Tafel slope [mV dec^{-1}]
Birnessite	0.00	0.0004	2.0	243 ± 7
Ni^{2+}/Birnessite	6.1	0.031	24	72 ± 4
Ni^{2+}/Birnessite	6.5	0.056	43	65 ± 3
Ni^{2+}/Birnessite	7.7	0.061	46	60 ± 3
β-NiOH$_2$	N/A	0.0036	2.5	105 ± 4

mass activities. Interestingly, we found that Ni^{2+}/birnessite exhibited a higher TOF (0.03–0.06 s^{-1} at $\eta = 400$ mV) than β-$Ni(OH)_2$ nanosheets (0.003 s^{-1} at $\eta = 400$ mV). This tenfold increase in TOF for Ni^{2+}/birnessite showed that water oxidation catalysis can be improved if an active catalyst is confined to the interlayer region. Gaseous O_2 product was confirmed by gas chromatography (Figure S12). Chronopotentiometric experiments at constant current density of 5 mA cm^{-2} showed enhanced stability of Ni^{2+}/birnessite relative to birnessite (Figure S13). Ni^{2+}/birnessite was stable for over 4 hours, whereas birnessite was limited to minutes. To obtain further insight into the deactivation mechanism of the catalyst, we used Raman, TEM, and XPS to characterize the electrocatalyst ink before and after the OER (Figures S16 and S17). The Raman spectra suggested an electrochemically induced structural disorder in the catalyst. TEM images showed the presence of surface corrosion with electrochemical cycling. The XPS spectra showed a noticeable peak shift towards lower binding energy with increasing electrochemical cycles in both the Ni 2p and O 1s regions. This binding energy shift is attributed to a change in chemical environment of interlayer nickel ions where the initial Ni-hydroxide nature transforms at least partially to Ni-oxide. It is well known that metastable Ni-hydroxide can undergo a phase transformation to Ni-oxide with annealing,[28] thus it is reasonable to assume that a similar electrochemically induced phase transformation can occur to interlayer nickel with extensive redox cycling, and can lead to deterioration of the catalytic activity.

Molecular dynamics (MD) simulations were carried out to shed light on the enhanced catalytic activity of Ni^{2+}/birnessite. Free energy surfaces obtained from MD simulations (Figure 5), suggest that the barrier to electron transfer (ET) is significantly reduced in the interlayer region relative to the same process occurring in bulk solution. Thus, the activation barrier for ET to occur, that is, the overpotential, is expected
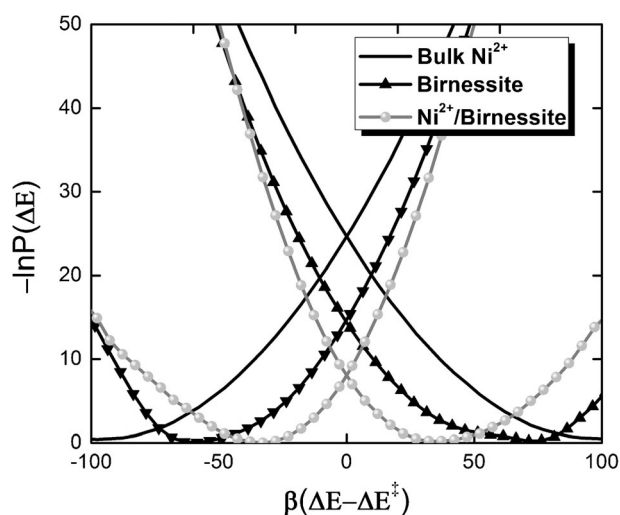

Figure 5. Free energies, $-\ln P(\Delta E)$, as a function of the energy gap, ΔE, which adequately quantifies electron transfer reactions, for the oxidized (left-most) and reduced (right-most) states of a model cation in bulk water and confined within the birnessite interlayer. Here, $\beta = 1/k_B T$, where k_B is Boltzmann's constant and T is the temperature. The curves are aligned vertically at their minima and horizontally at the location of the barrier, $\Delta E^{\ddagger}$. The free energetic barrier to electron transfer is lower when the reaction occurs in the birnessite interlayer and with Ni^{2+}.

to be smaller when the ion is confined within the interlayer. This contention is supported by the polarization curves (Figure 3) indicating that oxidation of Ni^{2+} to Ni^{3+} occurs at a lower potential when nickel is in the interlayer region of birnessite. In particular, Ni^{2+}/birnessite exhibits a feature at 1.37 V, while β-nickel hydroxide exhibits a peak at 1.44 V. The lowering of the barrier arises in part from a reduction in the number of reorganizing waters coordinated to the ion, from 6 to 4 moving from bulk water to birnessite. As predicted previously,[18] additional lowering of the barrier to ET in the interlayer arises from enhanced fluctuations owing to unique ion hydration structures which frustrate water molecules in neighboring cation hydration shells, and this structuring may facilitate the OER.[18]

MD simulations of Ni^{2+}/birnessite indeed suggest that interlayer water is highly ordered, and even more so than in standard potassium birnessite. In particular, Figure 6 depicts the probability distribution of water orientation for both Ni^{2+}/birnessite and potassium birnessite expressed as the angle made by a water dipole within the interlayer and the vector normal to the birnessite surface. In Ni^{2+}/birnessite, the probability of a water molecule to orient its dipole parallel to the surface is higher, in part due to the octahedral coordination structure of Ni^{2+} ions (Figure 6b). Moreover, water molecules are far less likely to adopt other orientations. Thus, the enhanced activity in Ni^{2+}/birnessite may be due to the confined interlayer environment and the resulting increase in orientational ordering of interlayer water that aids redox reactions.

In conclusion, the confinement of nickel hydroxide in the interlayer of birnessite resulted in a substantial enhancement of water oxidation catalysis. These results have broad implications for the synthesis of other active OER catalysts
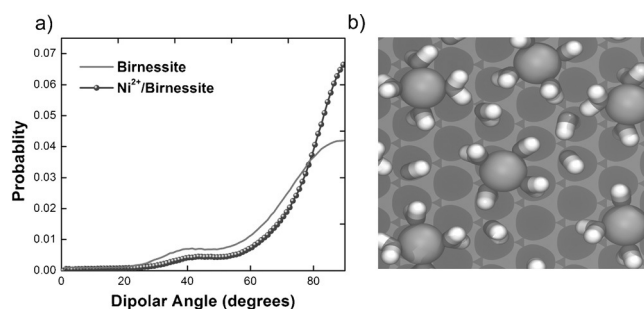
Figure 6. a) Probability distribution of the angle formed by a water dipole and the normal to the birnessite surface for birnessite and Ni²⁺/birnessite. Note that the angle is confined to be between 0 and 90 degrees owing to symmetry. b) Snapshots of water and ions in Ni²⁺/birnessite highlighting the orientational ordering of water and the octahedral coordination of Ni²⁺ (4 waters and 2 birnessite oxygens). See Figure S21 for colored image.

exploiting confinement within layered or nano-porous materials.

[1] A. J. Bard, M. A. Fox, *Acc. Chem. Res.* **1995**, *28*, 141.
[2] M. W. Kanan, D. G. Nocera, *Science* **2008**, *321*, 1072.
[3] H. B. Gray, *Nat. Chem.* **2009**, *1*, 7.
[4] T. R. Cook, D. K. Dogutan, S. Y. Reece, Y. Surendranath, T. S. Teets, D. G. Nocera, *Chem. Rev.* **2010**, *110*, 6474.
[5] J. K. Hurst, *Science* **2010**, *328*, 315.
[6] M. G. Walter, E. L. Warren, J. R. McKone, S. W. Boettcher, Q. Mi, E. A. Santori, N. S. Lewis, *Chem. Rev.* **2010**, *110*, 6446.
[7] M. T. M. Koper, *J. Electroanal. Chem.* **2011**, *660*, 254.
[8] K. Jin, J. Park, J. Lee, K. D. Yang, G. K. Pradhan, U. Sim, D. Jeong, H. L. Jang, S. Park, D. Kim, N.-E. Sung, S. H. Kim, S. Han, K. T. Nam, *J. Am. Chem. Soc.* **2014**, *136*, 7435.
[9] C.-H. Kuo, I. M. Mosa, A. S. Poyraz, S. Biswas, A. M. El-Sawy, W. Song, Z. Luo, S.-Y. Chen, J. F. Rusling, J. He, S. L. Suib, *ACS Catal.* **2015**, *5*, 1693.
[10] I. G. McKendry, S. K. Kondaveeti, S. L. Shumlas, D. R. Strongin, M. J. Zdilla, *Dalton Trans.* **2015**, *44*, 12981.
[11] Y. Meng, W. Song, H. Huang, Z. Ren, S.-Y. Chen, S. L. Suib, *J. Am. Chem. Soc.* **2014**, *136*, 11452.
[12] M. M. Najafpour, F. Rahimi, E.-M. Aro, C.-H. Lee, S. I. Allakhverdiev, *J. R. Soc. Interface* **2012**, *9*, 2383.
[13] A. C. Thenuwara, S. L. Shumlas, N. H. Attanayake, E. B. Cerkez, I. G. McKendry, L. Frazer, E. Borguet, Q. Kang, M. J. Zdilla, J. Sun, D. R. Strongin, *Langmuir* **2015**, *31*, 12807.
[14] J. E. Post, *Proc. Natl. Acad. Sci. USA* **1999**, *96*, 3447.
[15] M. Villalobos, B. Toner, J. Bargar, G. Sposito, *Geochim. Cosmochim. Acta* **2003**, *67*, 2649.
[16] B. M. Tebo, J. R. Bargar, B. G. Clement, G. J. Dick, K. J. Murray, D. Parker, R. Verity, S. M. Webb, *Annu. Rev. Earth Planet. Sci.* **2004**, *32*, 287.
[17] S. M. Webb, B. M. Tebo, J. R. Barger, *Geomicrobiol. J.* **2005**, *22*, 181.
[18] R. C. Remsing, I. G. McKendry, D. R. Strongin, M. L. Klein, M. J. Zdilla, *J. Phys. Chem. Lett.* **2015**, *6*, 4804.
[19] M. Gao, W. Sheng, Z. Zhuang, Q. Fang, S. Gu, J. Jiang, Y. Yan, *J. Am. Chem. Soc.* **2014**, *136*, 7077.
[20] X. Xia, H. Li, Z. H. Chen, *J. Electrochem. Soc.* **1989**, *136*, 266.
[21] D. Chen, D. Ding, X. Li, G. H. Waller, X. Xiong, M. A. El-Sayed, M. Liu, *Chem. Mater.* **2015**, *27*, 6608.
[22] Y.-K. Hsu, Y.-C. Chen, Y.-G. Lin, L.-C. Chen, K.-H. Chen, *Chem. Commun.* **2011**, *47*, 1252.
[23] C. Julien, M. Massot, R. Baddour-Hadjean, S. Franger, S. Bach, J. P. Pereira-Ramos, *Solid State Ionics* **2003**, *159*, 345.
[24] H. W. Nesbitt, D. Legrand, G. M. Bancroft, *Phys. Chem. Miner.* **2000**, *27*, 357.
[25] T. Shinagawa, A. T. Garcia-Esparza, K. Takanabe, *Sci. Rep.* **2015**, *5*, 13801.
[26] Y. Li, L. Jiang, F. Liu, J. Li, Y. Liu, *RSC Adv.* **2014**, *4*, 24020.
[27] L. Trotochaud, J. K. Ranney, K. N. Williams, S. W. Boettcher, *J. Am. Chem. Soc.* **2012**, *134*, 17253.
[28] Z.-H. Liang, Y.-J. Zhu, X.-L. Hu, *J. Phys. Chem. B* **2004**, *108*, 3488.